LIP-STUDENTS-24-10

Gas detectors R&D

Fernando Lopes[1,a] and Joao Simoes[1,b]

[1] *LIP - Laboratorio de Instrumentacao e Fisica Experimental de Particulas, Coimbra, Portugal*

Project supervisors: Dra. Filomena Santos, Afonso Marques

November 20, 2024

Abstract. This work, in the context of the LIP summer internship program, aims to report on the experiments performed with various gas detectors. The working principles of the detectors were explained and the data obtained was thoroughly analyzed in order to reach certain experimental conclusions, which were then compared with the theoretical predictions.

KEYWORDS: XENON, DRIFT, SCINTILLATION, CENTROID,FLUORESCENCE

1 Introduction

Over the last few decades, the interest in gas detectors has been renewed, given their versatility when compared to their liquid and solid-state counterparts. They are highly customizable in size, pressure, shape and gas filling. These customization options allow gas detectors to meet the most diverse of needs, particularly in particle physics, X-ray spectrometry, X-ray astronomy and medical instrumentation [1] [2].

1.1 Physical phenomena in noble gases

When a particle travels through a gas, several processes of energy transfer can occur. In the case of noble gases, given that the atoms possess neither vibrational nor rotational modes through which they can lose energy, the particle can, at first, collide elastically with the gas atoms. Depending on the energy of the particle, other processes, such as excitation and ionization, can take place. The former, which requires lower energies, consists of the transfer of an electron from a layer of lower energy to one of a higher energy. The subsequent collision with the gas atoms forms an excited dimer, which decays to the ground state, emitting photons of a characteristic energy.

$$\begin{array}{rcl} e^- + Xe & \rightarrow & Xe^\star \\ Xe^\star + 2Xe & \rightarrow & Xe_2^\star + Xe \\ Xe_2^\star & \rightarrow & 2Xe + h\nu \end{array} \tag{1}$$

On the other hand, if a particle has enough energy, it can remove electrons from the gas atoms which, in the absence of an electric field, recombine with the resultant ions, emitting a characteristic light signal. These two light-emitting processes by excitation and recombination are know as primary scintillation because they are related to the primary interaction event. Usually, the signal produced is small and hard to detect, but it has been used in rare-event experiences, in which the position and instant of these events are unknown. One example of such an experiment is the NEXT collaboration, which aims to search for the neutrinoless double beta decay in Xe-136, a process that has never been detected but that would allow to confirm the nature of the neutrino, namely, that it is a Majorana particle, using high-pressure gas electroluminescent time projection chambers [3].

$$\begin{array}{rcl} e^- + Xe & \rightarrow & Xe^+ + 2e^- \\ Xe^+ + Xe & \rightarrow & Xe_2^+ \\ Xe_2^+ + e^- & \rightarrow & Xe^{\star\star} + Xe \\ Xe^{\star\star} & \rightarrow & Xe^\star + h\nu \end{array} \tag{2}$$

In the presence of an electric field, the electrons produced in ionization can acquire enough energy to excite the atoms of the gas, producing a characteristic light signal in a process identical to excitation in primary scintillation. In this case, the number of photons emitted is higher compared to the previous process, and it depends on the applied electric field and on the gas (or gas mixture). This process is known as secondary scintillation (or electroluminescence).

The number of photons, reduced to the gas pressure, in this process (or, in another words, the light gain) has a linear dependence on the reduced electric field E/p:

$$\frac{Y}{p} = A \cdot \left(\frac{E}{p}\right) + B \tag{3}$$

where A and B are constants characteristic of the gas in study.

The secondary scintillation process has lower statistical fluctuations when compared with more energetic processes.

1.2 Fluorescence

Fluorescence is a short-lived photoluminescence process, triggered by irradiation of a substance with light. The light hitting a sample puts atoms, ions or molecules into excited states, from which they decay into lower energy states, emitting fluorescence photons. Each element has a specific fluorescence profile and so, the analysis of this light allows for the identification of such an element.

[a] e-mail: fernandogl20042@gmail.com

[b] e-mail: jpsimoes03@hotmail.com

2 Gas Proportional Scintillation Counter (GPSC)

2.1 Objective

Given the abundance of secondary scintillation values for pure Xenon gas in the literature, this experiment merely aims to replicate those results using a pressure of approximately 800 Torr.

2.2 Experimental setup

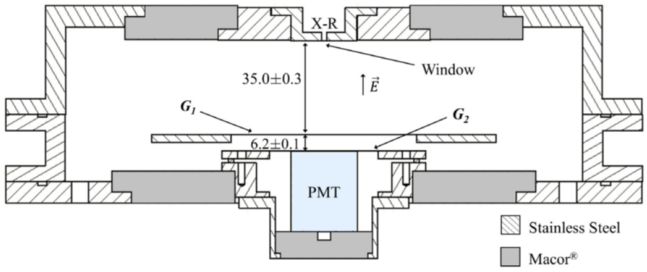

Figure 1. GPSC schematic; X-R: X-rays entrance, G1 and G2: metallic grids that define the drift and scintillation regions, PMT: photomultiplier tube [4].

The experimental setup used in this study is represented in Figure 1. The detector consists of a cylindrical stainless-steel vessel 70 mm high and with a diameter of 240 mm. This chamber is filled with the gas under study through tubes connected to a gas circulation (three resistors at 120 $^{\circ}C$ that promote the circulation) and purification system (MicroTorr MC1-702F purifier). The radiation entrance window has a 1 mm diameter and is covered with a 200 nm aluminum film in the detector's inner side, to allow electrical contact with the detector's top flange, ensuring that the electric field near the entrance window is uniform [4].

Inside the detector there are two parallel metallic grids (G1 and G2) which define two electric field regions: the drift region, 35.0 ± 0.3 mm deep, localized between the entrance window and G1, in which the electrons are accelerated, and the scintillation region, 6.2 ± 0.1 mm deep, between G1 and G2, where the phenomenon under study occurs. G2 is kept at ground potential, while the window and G1 are biased with negative electric potentials. The voltages are supplied by a CAEN N1470 high voltage power supply [4] that is controlled by a computer via USB interface.

The electroluminescence signal produced is detected by a photomultiplier tube (PMT), Hamamatsu R8520-406 PMT, and is amplified through a Tennelec TC243 amplifier and fed to an Amptec MCA8000D multichannel analyzer [4].

The radioactive source used is Co-57, which, through electron capture, emits X-rays with energies of roughly 6.5 and 7.0 keV that correspond respectively to the K_α and K_β. Other photon emissions occur at higher energies, but are mostly irrelevant for this study. Additionally, a lead collimator was used to narrow the beam of X-rays [4].

2.3 Experimental preparation

For this experiment, values for the drift pressure-reduced electric field, $(\frac{E}{p})_d$, varied between 0.3 and 0.8 V cm^{-1} Torr^{-1} in intervals of 0.1 V cm^{-1} Torr^{-1}, and, for each value of $(\frac{E}{p})_d$, the scintillation pressure-reduced electric field, $(\frac{E}{p})_c$, usually took values between 3.0 and 9.0 V cm^{-1} Torr^{-1}, in intervals of 0.5 V cm^{-1} Torr^{-1}.

The electric fields mentioned above have the following relation with the voltages of the grids, where V_g is the G1 voltage, V_j is the window voltage, d_c is the scintillation region distance, d_d is the drift region distance and p is the pressure inside the detector:

$$\begin{aligned} V_g &= \left(\frac{E}{p}\right)_c \cdot p \cdot d_c \\ V_j &= \left(\frac{E}{p}\right)_d \cdot p \cdot d_d + V_g \end{aligned} \tag{4}$$

2.4 Experimental run

The number of photons detected with a given energy were read as a spectrum in the program Amptek DppMCA, using a resolution of 512 channels. For the vast majority of the runs 2 energy peaks were detected, but, it should be noted that for higher values of the scintillation electric field, the second peak was harder to distinguish from the background noise.

A few runs were performed with slight alterations to understand their impact on the results. One run was performed with 1024 channels, instead of 512, and a shift in the peaks' positions was observed. Another run was performed with the amplification value doubled (from 5 to 10), and one of the peaks could no longer be observed. Finally, one run was performed with half the acquisition time (from 1s to 500 ms), and no change was observed.

2.5 Results and data analysis

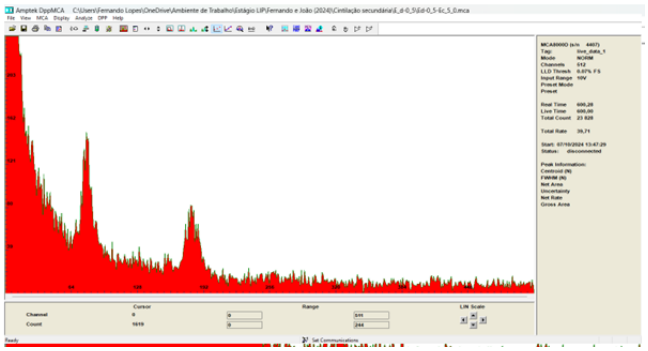

Figure 2. Example of the spectra obtained from the GPSC ($(\frac{E}{P})_d$ = 0.5 V cm^{-1} Torr^{-1}, $(\frac{E}{P})_c$ = 5,0 V V cm^{-1} Torr^{-1})

Before analysing the obtained spectra, an explanation of their particular shape is necessary.

The radioactive source emits radiation through the following processes:

$$\begin{aligned} {}^{57}_{27}\mathrm{Co} + e^- \rightarrow {}^{57}_{26}\mathrm{Fe}^* p + e^- \rightarrow n + \nu_e \\ {}^{57}_{26}\mathrm{Fe}^* \rightarrow {}^{57}_{26}\mathrm{Fe} + \gamma \end{aligned} \quad (5)$$

The second process is responsible for the emission of the X-rays (K_α = 6.4 keV and K_β = 7.0 keV) which ionize xenon atoms and the electrons originated are accelerated in the drift region, which then cause the secondary scintillation signal explained previously. Given the height of the first peak and the proximity in value of K_α and K_β, it is fairly safe to assume that the former corresponds to these two energy values and the detector just doesn't have the required resolution to distinguish them.

Regarding the second peak, it may stem from fluorescence processes in the lead collimator. It should be noted that the "peak" near the 0 channel corresponds to electronic noise.

To find each clear-cut peak, the built-in gaussian analysis tool of the software was used. Given a selected region of data, the tool provided the centroid (the channel of the peak) and the full width at half maximum (FWHM) of the gaussian. Using the data collected, two representations were used:

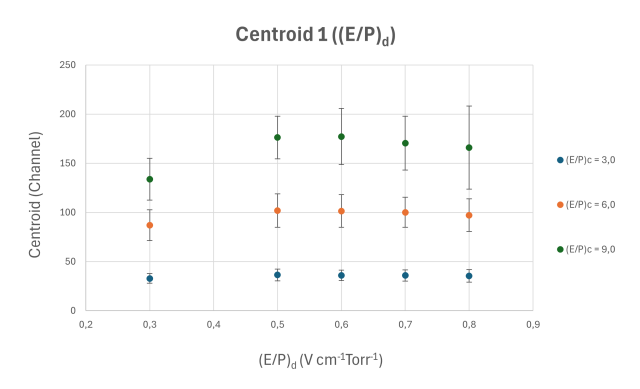

Figure 3. Centroid of the first peak with respect to the reduced drift field while holding the scintillation field constant at 3.0, 6.0 and 9.0 V cm^{-1} Torr^{-1}.

A brief overview of Figure 3 suggests that, given a certain value of the scintillation field, the energy associated with the first peak appears to rise until a value of 0.5 V cm^{-1} Torr^{-1} for the drift field, after which it remains fairly constant. Furthermore, Figure 4 also suggests that the drift field has little impact on the value of the first peak and that this value appears to have a linear relation with the scintillation field. This was also confirmed by performing 3 linear projections whose values of the coefficient of determination (r^2) are all close to the desired value of 1.

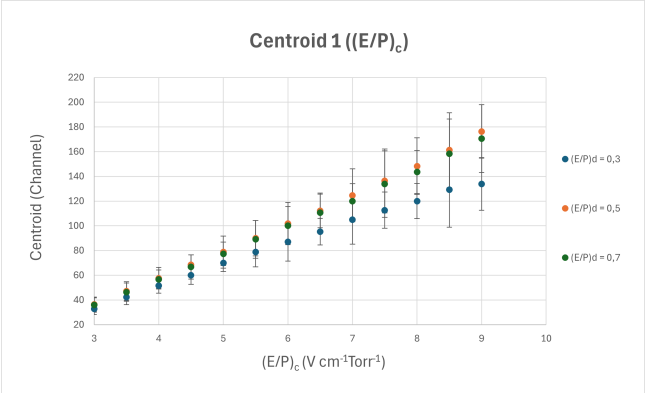

Figure 4. Centroid of the first peak with respect to the reduced scintillation field while holding the drift field constant at 0.3, 0.5 and 0.7 V cm^{-1} Torr^{-1}.

m	17,12	-16,7296	b
u(m)	0,22	1,41	u(b)
r^2	0,998	1,51	u(Centroid)

Figure 5. Matrix of the linear projection of Centroid of the first peak with respect to the reduced scintillation field while holding the drift field constant at 0.3 V cm^{-1} Torr^{-1}.

m	22,97	-34,8602	b
u(m)	0,29	1,84	u(b)
r^2	0,998	1,97	u(Centroid)

Figure 6. Matrix of the linear projection of Centroid of the first peak with respect to the reduced scintillation field while holding the drift field constant at 0.5 V cm^{-1} Torr^{-1}.

m	22,23	-32,71	b
u(m)	0,27	1,67	u(b)
r^2	0,998	1,80	u(Centroid)

Figure 7. Matrix of the linear projection of Centroid of the first peak with respect to the reduced scintillation field while holding the drift field constant at $0,7 Vcm^{-1}Torr^{-1}$

2.6 Conclusions

The results regarding the drift field are not surprising. When low drift fields are applied, some of the electrons suffer recombination instead of drifting to the scintillation region, thus resulting in a lower value for the centroid of the first peak. When this field reaches a certain value, all electrons are drifted and no recombination occurs. Given that all values for the drift field are lower than those of the scintillation field, no change in the value of the centroid is expected for higher values of the former.

The results for the scintillation field are in good agreement with the ones found in the literature, not only for

similar experiments using similar detectors, but also for Monte Carlo and Boltzmann simulations for room temperature (See [5]).

3 Cylindrical Proportional Counter

3.1 Objective

The purpose of this experiment is to establish a relationship between the channels presented in the Amptek DppMCA program and the energy with which they are associated by using known values of K_α and K_β emission for different elements.

3.2 Experimental setup

The radioactive source used was a small alpha particle source. The various metallic targets were hit with these particles which excited the samples in a characteristic way, leading to emissions of K_α and K_β X-rays. The detector used for the study of these emissions consists of a cathode (an outer cylinder) and an anode, which establish an electric field inside the detector. The incident X-rays are responsible for ionizing the gas inside and the electric field accelerates them towards the anode, where they are collected. The signal is then pre-amplified and amplified, before finally reaching the Amptec MCA8000D multichannel analyzer. The signal is then read as a spectrum in the Amptek DppMCA program.

3.3 Experimental preparation

The voltage between the cathode and anode took two values: 900 and 1000 V. The following metallic targets were used: Ba, Cr, Cu, Mn, Ni, Pb, Sn, Ti, W, Zn, a coin and a mixture of unknown composition.

3.4 Experimental run

The signal was once again read as a spectrum in the Amptec DppMCA program using a resolution of 512 channels. For the vast majority of the runs, only one peaked was observed.

3.5 Results and data analysis

Similarly to the GPSC experiment, the detector does not have enough resolution to distinguish the peaks associated with the K_α and K_β X-ray emissions so, it is safe to assume, that the peak observed corresponds to these processes. Using values for the energies associated with these emissions, as well as for their relative abundance, the following relation between the energy in keV and the channel number was found.

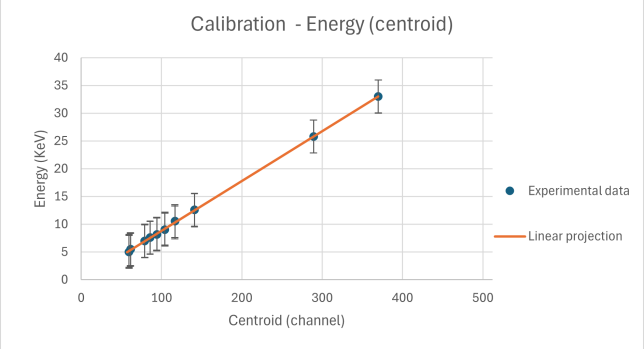

Figure 8. Energy of the X-ray emissions versus the peak's centroid

As observed in Figure 8, the energy is proportional to the channel number and a linear projection was made in order to confirm this observation.

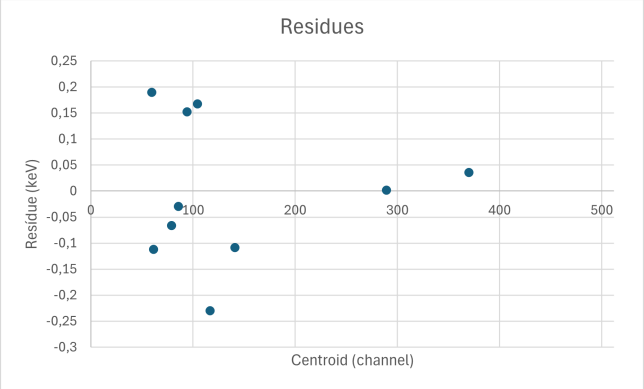

Figure 9. Residues associated with the linear projection.

m	0,08970	-0,14734	b
u(m)	0,00047	0,07996	u(b)
r^2	0,9998	0,146	u(E)

Figure 10. Matrix of the linear projection.

Given that none of the residue values are greater than $2u(E)$ and the value of r^2 so close to 1, it is safe to assume that the linear projection is adequate. Additionally, the values of b, the intersection of the graph with the y-axis is very close to zero, which is to be expected.

The results for the 1000 V voltage were very similar.

3.6 Conclusions

Given all that was stated above, the energy in keV and the channel number are related through the following equation:

$$E = 0.08970 \times \text{Channel} - 0.14734 \quad \text{(keV)} \quad (6)$$

The similar results for the 1000 V are not surprising, given that the voltage, and thus the electric field, only affect the acceleration of the electrons towards the anode, and not the number of electrons produced by each ionization of the gas atoms.

Finally, using the reference values, it is estimated that the coin is made out of copper and that the mixture is composed primarily of Manganese.

4 Results and Conclusions

Both experiments described in this report were successful in achieving the objectives that were initially laid out. The results are in agreement with the literature and we were able to familiarize ourselves with the workings of these two gas detectors, as well as a few others which were not included in this report.

Acknowledgements

We would like to thank our project supervisor Dr. Filomena and all the faculty, researchers and students at LIP for their support throughout this internship. However, we would like to especially acknowledge Afonso Marques. Without his guidance and total availability, the completion of the experiments would have been impossible. His helpfulness and friendliness were absolutely instrumental to the smooth course of the internship. To him go our deepest thanks.

References

[1] A. Trindade, J. Escada, M.R. Silva, A. Marques, F. Borges, F. Santos, Nuclear Instruments and Methods in Physics Research Section A: Accelerators, Spectrometers, Detectors and Associated Equipment **1049**, 168038 (2023)

[2] A.M.F. Trindade, J. Escada, J.M. Maia, R.M. Curado da Silva, A.P. Marques, F.P. Santos, IEEE Transactions on Nuclear Science **70**, 254 (2023)

[3] P. Novella, M. Sorel, A. UsÃşn, C. Adams, H. AlmazÃąn, V. ÃĄlvarez, B. Aparicio, A.I. Aranburu, L. Arazi, I.J. Arnquist et al., Journal of High Energy Physics **2023** (2023)

[4] A.M. da Fonseca Trindade, Ph.D. thesis, Universidade de Coimbra (2022)

[5] C.M.B. Monteiro, L.M.P. Fernandes, J.A.M. Lopes, L.C.C. Coelho, J.F.C.A. Veloso, J.M.F. dos Santos, K. Giboni, E. Aprile, Journal of Instrumentation **2**, P05001 (2007)